ScienceDirect

Download

Journal of Membrane Science
Volume 598, 15 March 2020, 117660

Fluorine-containing polyimide/polysilsesquioxane carbon molecular sieve membranes and techno-economic evaluation thereof for C_3H_6/C_3H_8 separation

Ju Ho Shin [a, 1], Hyun Jung Yu [a, 1], Junhyung Park [a, 1], Albert S. Lee [b], Seung Sang Hwang [b], Seok-Jhin Kim [c], Sunghwan Park [a], Kie Yong Cho [a], Wangyun Won [d], Jong Suk Lee [a]

Show more

Outline | Share Cite

https://doi.org/10.1016/j.memsci.2019.117660

Get rights and content

Highlights

- Fluorinated polyimide/ladder-like polysilsesquioxane CMS membranes were investigated for C_3H_6/C_3H_8 separation.
- Thermo-oxidative crosslinking and partial etching of LPSQ formed impermeable silica phases.
- Embedded silica in the carbon matrix enhanced effective ultramicropores for C_3H_6/C_3H_8 separation efficiency.
- CMS membranes showed C_3H_6/C_3H_8 selectivity of 67 from enhanced diffusivity selectivity.
- Techno-economic analyses showed economic feasibility of a membrane-distillation hybrid process.

Abstract

Herein, we investigated the effect of thermo-oxidative crosslinking of siloxanes on the C_3H_6/C_3H_8 separation performance of carbon molecular sieve (CMS) membranes derived from polymer blends of a fluorine-containing polyimide and a ladder-structured polysilsesquioxane (PI/LPSQ). The PI/LPSQ precursors self-generated fluorinated gases, which possibly lead to the cleavage of double-stranded siloxanes during pyrolysis. At the same time, residual siloxanes underwent thermo-oxidative crosslinking, which resulted in densification into nonporous inorganic SiO_2 phases. Such impermeable SiO_2 phases adversely affected the gas diffusion, decreasing C_3H_6 permeability but contributed to the significant enhancement in the C_3H_6/C_3H_8 selectivity up to as much as 67, because of the substantially enhanced diffusivity selectivity. Density functional theory-based pore size distribution analysis exhibited that the narrower pores in the range of 5.0–5.5 Å emerged for the PI/LPSQ (8

FEEDBACK

supporting the enhancement in C_3H_6/C_3H_8 selectivity. Also, PI/LPSQ (80/20 w/w) CMS fibers aged for 30 days showed C_3H_6 permeance of 2.9 GPU and a C_3H_6/C_3H_8 selectivity of 57. Furthermore, the techno-economic analysis verified the economic feasibility of the proposed membrane for the C_3H_6/C_3H_8 separation process. It reflected that higher C_3H_6 permeability plays a significant role in reducing the total cost of C_3H_6/C_3H_8 separation process as long as the C_3H_6/C_3H_8 selectivity is above 30, implying the significance of anti-aging in CMS hollow fiber membranes.

Graphical abstract

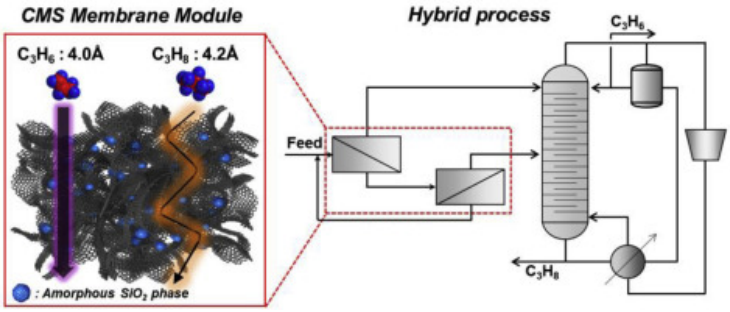

Download : Download high-res image (301KB) Download : Download full-size image

Previous Next

Keywords

Carbon molecular sieve membranes; Thermo-oxidative crosslinking; Siloxane; C_3H_6/C_3H_8 separation efficiency; Techno-economic evaluation

1. Introduction

A promising membrane in challenging gas separations can be realized through development of carbon molecular sieve (CMS) membranes because of their peculiar bimodal pore structures [1,2]. These peculiar pore structures of CMS membranes can be tuned by the effect of pyrolysis protocol, pyrolysis atmosphere and pre/post treatments [3,4]. The pyrolysis protocol is determined by parameters including the final soaking temperature, soaking times, and ramp rates. The higher soaking temperatures and longer soaking times during pyrolysis are known to cause a decrease in the size of micropore and ultramicropores, resulting in an increase in selectivity and a decrease in permeability [5]. The pyrolysis atmosphere can be controlled by using various types of purge gases. Most notably, engineering the size of ultramicropores via oxygen doping during pyrolysis is an effective method to enhance selectivity [6,7]. Pre/post treatments refer to additional steps that are taken following a precursor membrane fabrication [8]. Richter et al. demonstrated that by performing post-pyrolysis oxygen treatments on CMS membranes, the transport mechanism is changed from a molecular sieving process to a selective surface flow [9].

Meanwhile, engineering novel polymer precursor is also critical to achieve desirable pore structures in CMS membranes for high separation performance. Chu et al. showed that polyimides containing iron complexes show enhanced olefin affinity, resulting in higher olefin/paraffin selectivity [10]. Furthermore, CMS membranes derived from an intrinsically microporous polyimide showed a superior ethylene/ethane selectivity as well as a high ethylene permeability because the collapse of the microporous structure was hindered [11]. Additionally, CMS derived from polymers of intrinsic microporosity (PIM) with beta-cyclodextrin showed a slight increase in propylene permeability and propylene/propane selectivity compared to those derived from the untreated PIM membrane [12]. Other groups have fabricated carbon-zeolite composite membranes in order to combine the advantages of high separation capability as well as chemical/thermal stability [13,14]. These approaches, however, lacked the fabrication of zeolites with pore sizes perfectly fit for separation of gases with miniscule size differen

FEEDBACK

introduced a series of carbon-silica (C–Si) composite membranes, where the continuous carbon matrix behaves as a molecular sieve while the dispersed SiO_2 domains enhanced productivity [15]. Unfortunately, their approach was inappropriate for high C_3H_6/C_3H_8 selectivity, albeit substantially improving C_3H_6 permeability.

Recently, our group demonstrated the fabrication of CMS hollow fiber membranes with a thin selective layer, which was derived from a hybrid polymeric precursor containing a polyimide and a ladder-structured polysilsesquioxane [16]. The rigid double-stranded siloxane backbone suppresses thermal relaxation during pyrolysis, allowing the preparation of highly productive CMS hollow fiber membranes. This has prompted us to explore the effect of LPSQ addition on the olefin/paraffin separation performances of the hybrid CMS membranes.

Here, we investigated the effect of thermo-oxidative crosslinking of siloxanes on the C_3H_6/C_3H_8 separation efficiency of CMS membranes derived from a fluorinated PI. The Koros group reported the V-treatment process, which involves the coating of vinyltrimethoxysilane to be used for the suppression of substructure collapse in CMS membranes [17]. While thermo-oxidative crosslinking of siloxanes in CMS membranes is also seen in V-treatment, the excess silica from V-treatment simply acted as an additional resistive layer without enhancing the gas selectivity [17,18]. However, the siloxane components in our CMS membranes may behave as an impermeable dispersed phase in the amorphous CMS matrix, possibly generating a tortuous path for larger penetrants. CO_2 physisorption and TEM analysis was employed to characterize the CMS membranes derived from polyimide/polysilsesquioxane dense films. Furthermore, the C_3H_6/C_3H_8 single gas separation performance and equimolar mixed gas separation performance of CMS membranes as a function of polysilsesquioxane content was evaluated. In addition, the C_3H_6/C_3H_8 single gas separation performance of hybrid CMS hollow fiber membranes were studied in order to evaluate the economic feasibility of membrane processes involving such materials.

2. Experimental

2.1. Materials

6FDA-DAM:DABA (3:2) (PI) polymers and ladder structured-poly (phenyl-co-pyridylethyl)silsesquioxane with phenyl: pyridylethyl ratio of 6:4 (LPPyr64), LPSQ was synthesized in-house as described in our previous work [16]. Single gases of CO_2, N_2, CH_4, C_3H_6, C_3H_8 (purity of 99.999%) and equimolar C_3H_6/C_3H_8 mixed gases were purchased from MS Gas Corporation.

2.2. Fabrication of precursor dense film membranes

LPSQ and PI were dissolved in THF at 5 wt% concentration, and the dope solution was mixed on a roller overnight. Filtration was performed using cotton pieces for removal of impurities after the dope solutions were completely dissolved. Film casting was conducted using Teflon-casting-rings on the Teflon plate in a THF saturated glove bag. After 12 h, the casted films were then dried at 120 °C for 12 h under a reduced pressure for complete dryness. As prepared films were fabricated for proper sized membranes using a sharp die cutter, yielding uniform films with a thickness of 80 ± 5 μm.

2.3. Fabrication of precursor hollow fiber membranes

PI/LPSQ (80/20 wt/wt) asymmetric hollow fiber membranes were fabricated using the same protocol reported in our previous work [16]. Hollow fiber membranes were fabricated using the dry-jet/wet-quench process, and the binodal curve was constructed using the cloud point technique prior to spinning [19]. The polymer dope solution consisted of PI and LPSQ as the polymer mixture, NMP and THF as the solvent, and $LiNO_3$ and EtOH as the non-solvent. The spinning dope solution was mixed on a roller until the solution became completely homogeneous. The extruded hollow fibers were removed from the take-up drum and underwent solvent exchange with DI water for 3 days, and they were finally washed with MeOH and hexane, in order. The outer diameter and inner diameter of the precursor hollow fiber membrane were 320 μm and 150 μm, respectively.

2.4. Fabrication of CMS membranes

All CMS membranes in this work were fabricated by pyrolyzing precursor polymeric films and hollow fibers with a similar protocol reported in our previous work [16]. Briefly, the precursor polymeric films were placed on a quartz plate and placed in the middle of a quartz tube. A three-zone furnace (Thermcraft, USA) with three separated thermocouples connected to a multi-channel thermo controller (Omega, USA) was used for the pyrolysis procedure. The quartz tube was purged by UHP Ar during pyrolysis, at a flow rate of 400 cm^3/min, which was controlled by a mass flow controller (MKP, Korea). The oxyge

FEEDBACK

was monitored by an oxygen analyzer (Cambridge Sensotec Ltd, UK). It must be noted that the pyrolysis of fluorinated polymers produces small amounts of hydrofluoric acid, which is highly corrosive, extremely toxic and can cause blindness upon contact with the eyes. For safety considerations, it is recommended that the gas effluent should be diluted by a continuous argon feed and neutralized with a dilute aqueous base solution prior to being vented to prohibit potential exposure to HF. After each pyrolysis run, the quartz tube and quartz plate were rinsed with acetone and purged with air at 800 °C. PI and PI-LPSQ membranes were pyrolyzed at 675 °C, following a well-known pyrolysis protocol. The membranes were heated from 50 to 250 °C at 10 °C min^{-1}, then to 660 °C at 3.85 °C min^{-1}, and to 675 °C at 0.25 °C min^{-1}. After soaking at 675 °C for 2 h, the furnace was naturally cooled down under argon purge. The outer diameter and inner diameter of CMS PI/LPSQ (80/20 wt/wt) hollow fiber membranes were 220 μm and 115 μm, respectively.

2.5. Supplementary characterization

Scanning transmission electron microscopy (STEM) of CMS membranes was conducted using a high-angle annular dark field scanning-TEM (HAADF-STEM) with Sc-connector on a FEI Titan 80–300 electron microscope. The accelerating voltage of the electron beam was 300 KeV and the scanning electron beam size was around 0.1 nm. The bulk density of CMS membranes was determined by helium pycnometer (AccuPyc 1340 (Micromeritics)). Pore distribution of CMS membrane was observed by CO_2 adsorption (ASAP 2020 (Micromeritics)) and calculated with density functional theory (DFT) [20]. The experiments were performed at 273.15 K at the absolute pressure range of 1–800 mmHg. Equilibrium sorption isotherms for C_3H_6 and C_3H_8 in CMS membranes were measured at 35 °C [21].

3. Results & discussion

3.1. Characterization of the micropore structure of CMS PI-LPSQ dense film membranes

6FDA-DAM:DABA (3:2) was the fluorinated polyimide used as a precursor for the blending approach incorporating ladder structured-poly (phenyl-co-pyridylethyl)silsesquioxane with phenyl:pyridylethyl ratio of 6:4 (LPPyr64), LPSQ to induce thermo-oxidative crosslinking during pyrolysis. The homogeneous blending of PI and LPSQ were achieved by the H-bonding between pyridyl sites in LPSQ and acid sites in PI. It was confirmed by the asymmetric carbonyl peak in the FT-IR spectrum, which exhibited an increase to a higher wavenumber [16]. The polymeric precursor membranes containing 0, 10, and 20 wt% LPSQ, respectively, were pyrolyzed at 675 °C to produce hybrid CMS membranes. The sample names for hybrid precursor and their CMS membranes were designated in the same manner as used in our previous work [16] by using the weight percentage of LPSQ in the blends, for instance, PI-LPSQ10 is comprised of 10 wt% of LPSQ and CMS PI-LPSQ10 is its carbonized analogue.

CO_2 physisorption experiments and density functional theory (DFT) calculations were employed to characterize pore size distribution of hybrid CMS membranes [1,22,23]. The DFT-based pore distribution spanned 4.0 Å to 11.0 Å, falling into the range of ultramicropores (<7 Å) and micropores (7–20 Å) [2]. Furthermore, as seen in Fig. 1a, narrower pores in the range of 5.0–5.5 Å emerged for CMS PI-LPSQ20. This is a critical region for effective sieving of C_3H_6/C_3H_8 separations, as one of the molecular length for both gases is in this pore size range (5.1 vs. 5.4 Å) [23]. The solid state ^{29}Si NMR spectra of CMS membranes reported in our previous work showed that the SiO_2 phases in the hybrid CMS membranes almost exclusively consist of Q^3 and Q^4 structures. Furthermore, cross sectional STEM images of the hybrid CMS membranes with EDX analysis show a morphology where impermeable SiO_2 remnants with an average size of 1 nm are uniformly incorporated into the carbon matrix (Fig. 1c-e and Fig. S1). From these observations, the reason for the preferential formation of well-defined, tuned ultramicropores as schematically depicted in Fig. 1b, was due to the homogeneous distribution of 1 nm sized SiO_2 scaffolds formed by thermo-oxidative crosslinking of LPSQ and the subsequent etching due to the evolution of HF/CHF_3 gases. The etching process should be associated with the bond energy. Since the bond energy of Si atoms to F- ions is stronger than that of Si to O (136 vs. 106 kcal/mol) [24,25], the etching process is most likely induced by HF/CHF_3 generated from hexafluoroisopropylidene groups in PI at close to 480 °C, which was confirmed from the TG-MS data reported in our previous work [16].

FEEDBACK

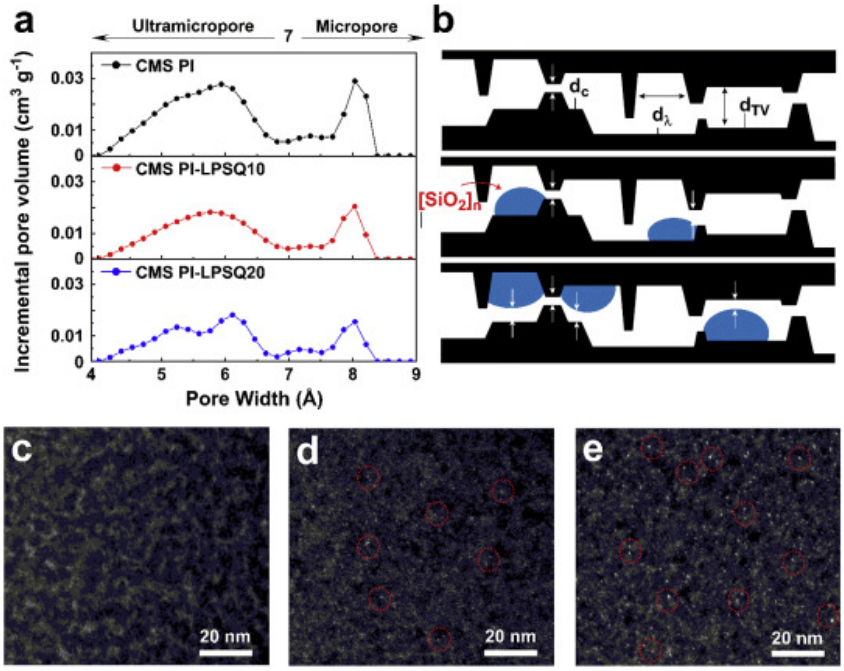

Download : Download high-res image (1MB) Download : Download full-size image

Fig. 1. Characterization of CMS membranes. (a) Pore size distribution of CMS membranes calculated by DFT model from CO_2 adsorption at 273 K. (b) Schematic cartoon of the potential pore structure of CMS membranes. TEM images of (c) CMS PI, (d) CMS PI-LPSQ10, (e) CMS PI-LPSQ20 membranes. The SiO_2 particles are indicated by the red eye-guiding circle. (For interpretation of the references to colour in this figure legend, the reader is referred to the Web version of this article.)

Fig. 2 illustrates the formation of our hybrid CMS membranes involving the thermo-oxidative crosslinking and etching of polysilsesquioxanes. As carbonization of a fluorine-containing polyimide/polysilsesquioxane blend precursors proceeds, (1) thermal degradation of polyimide as well as organic groups of polysilsesquioxane occurs, and immediately (2) thermo-oxidative crosslinking of remnant inorganics occurs, but (3) the hexafluoroisopropylidene groups in fluorine-containing polyimide generate fluorinated gases such as HF or CHF_3 [26,27], and (4) the fluorinated gases etch the majority of inorganic siloxane phases in polysilsesquioxane [28], and finally (5) the remaining small amorphous SiO_2 phases are homogeneously embedded in the turbostratic carbon network.

FEEDBACK

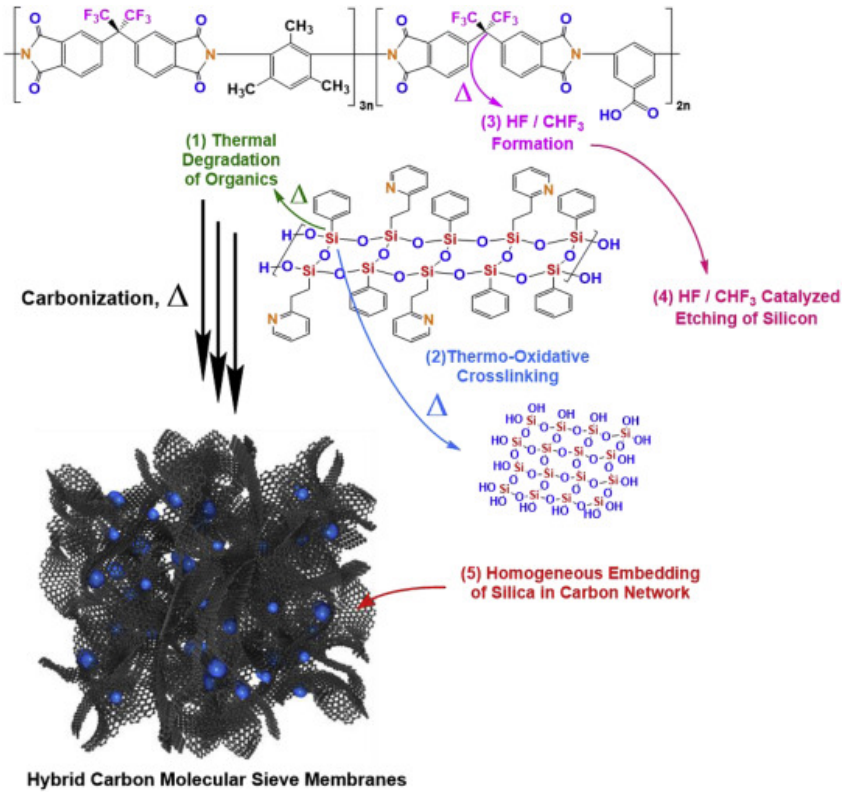

Download : Download high-res image (695KB) Download : Download full-size image

Fig. 2. Schematic for the formation of hybrid CMS membranes involving the thermo-oxidative crosslinking and etching of polysilsesquioxanes. The remaining silica phases are depicted as blue spheres. (For interpretation of the references to colour in this figure legend, the reader is referred to the Web version of this article.)

3.2. Single gas transport characterization of precursor PI-LPSQ membranes and CMS PI-LPSQ membranes

Single gas permeation tests of CO_2, N_2, CH_4, C_3H_6 and C_3H_8 were conducted at *ca.* 1 bar and 35 °C for our PI-based precursor membranes as well as their CMS counterparts (Table 1). The permeability values of the PI membrane for all examined gases were consistent with those reported previously [29]. Interestingly, the permeability of all light gases declined with increasing LPSQ concentration in polymer blends, while the polymer blends showed slightly higher permeability for both C_3H_6 and C_3H_8 than PI. Our previous work reported that LPSQ membranes showed poor penetrant size discrimination properties due to their large inter-chain distance, ca. 13 Å [30], and the diffusivity of all measured gases increased with LPSQ concentration (Table S1). Especially, the C_3H_6 and C_3H_8 diffusivity of the PI-LPSQ20 membrane increased by 46% and 70% compared to the neat PI membrane, respectively. Meanwhile, it should be noted that the increase in diffusivity of smaller gases (i.e., CO_2, N_2, CH_4) was less pronounced (6%, 2%, 27%) due to the weak size discrimination properties of LPSQ. Therefore, the inherently high diffusivity of LPSQ compared to PI increased the permeability of polymer blends for C_3H_6 and C_3H_8 but with some C_3H_6/C_3H_8 selectivity loss.

Table 1. Single gas permeation results of precursor dense film membranes and CMS dense film membranes at *ca.* 1 bar, 35 °C.

Sample	P_{CO2} [a)]	P_{N2} [a)]	P_{CH4} [a)]	P_{C3H6} [a)]	P_{C3H8} [a)]	$\alpha_{CO2/N2}$ (–)	$\alpha_{CO2/CH4}$ (–)	$\alpha_{C3H6/C3H8}$ (–)
PI	129 ±3	5.4 ±0.1	3.4 ±0.08	2.0 ±0.04	0.11 ±0.001	24 ±0.5	38 ±0.9	18 ±0.3

FEEDBACK

Sample	P_{CO2} [a)]	P_{N2} [a)]	P_{CH4} [a)]	P_{C3H6} [a)]	P_{C3H8} [a)]	$\alpha_{CO2/N2}$ (–)	$\alpha_{CO2/CH4}$ (–)	$\alpha_{C3H6/C3H8}$ (–)
PI-LPSQ10	117 ±4	4.7 ±0.1	3.3 ±0.05	2.1 ±0.02	0.14 ±0.004	25 ±0.7	36 ±1	15 ±0.1
PI-LPSQ20	92 ±3	3.9 ±0.1	3.0 ±0.1	2.1 ±0.1	0.17 ±0.01	23 ±0.7	30 ±1	12 ±0.5
LPSQ	34.2	1.3	2.8	4.4	1.6	26.7	12.4	2.8
CMS PI	3900 ±200	100 ±6	73 ±0.7	630 ±100	43 ±1	37 ±1	53 ±3	15 ±3
CMS PI-LPSQ10	2600 ±30	77 ±10	51 ±9	290 ±60	6.7 ±0.6	34 ±2	52 ±4	44 ±5
CMS PI-LPSQ20	1800 ±100	49 ±4	28 ±4	77 ±5	1.2 ±0.0	37 ±1	64 ±5	67 ±13

Note: The error bars in permeability were calculated using standard deviation of permeability in at least two separate samples. The error bars in selectivity were estimated using the propagation of uncertainty [32].

a Permeabilities in Barrer, where 1 Barrer = 10^{-10} cm^3(STP) cm cm^{-2} s^{-1} $cmHg^{-1}$.

However, for the hybrid CMS membranes, we saw an exceptional increase in C_3H_6/C_3H_8 separation efficiency as represented in Table 1. It should be noted that our CMS membranes were aged in vacuum for at least two weeks prior to characterization of gas transport to minimize effects of physical or chemical aging during transport characterization [16]. The CMS membranes stored in vacuum for over two weeks showed good reproducibility, while substantial permeability reduction was observed for those stored in air condition for the same time span due to the oxygen induced chemical aging (Fig. S2). As the amount of inorganic phase in CMS membranes increased, the permeabilities of both C_3H_6 and C_3H_8 decreased more drastically than that for other light gases used in this work (Table 1). The C_3H_6/C_3H_8 selectivity, however, showed a marked increase with increasing concentration of remnant inorganic phases in hybrid CMS membranes, while CO_2/N_2 and CO_2/CH_4 separations did not, implying that the additional ultramicropores formed by the arrangement of impermeable SiO_2 inside micropores are more suitable for C_3H_6/C_3H_8 separations. In addition, C_3H_6/C_3H_8 separation performances of both the pristine CMS membrane (CMS PI), and the hybrid CMS membrane (CMS PI-LPSQ20), either matched or surpassed those of previously reported CMS membranes. Such high C_3H_6 permeability seen in the pristine CMS membrane was attributed to the microvoids generated by thermal decarboxylation-induced crosslinking of DABA moieties in PI, which may be maintained during pyrolysis [26,31,44]. Moreover, the single gas permeabilities of CMS membranes were enhanced greatly compared to the precursor membranes. This phenomenon was especially pronounced for C_3H_6 and C_3H_8, whose permeability increased 315 times and 390 times, respectively after pyrolysis, in the case of the pristine CMS membrane. Chu et al. [10] also observed a drastic increase in C_3 permeability for their 6FDA-DAM:DABA (3:2) compared to the corresponding precursor analogue. Such sharp increase in the permeability of the C_3 gases was mainly due to the increase in diffusivity. Diffusion in polymeric membranes occurs from thermally activated movements of the polymer chains, and because the activation energy of diffusion tends to increase with penetrant size, the diffusivity of C_3H_6 and C_3H_8 was several orders of magnitude smaller than the smaller gases (i.e., CO_2, N_2, CH_4) (Table S1). On the other hand, CMS membranes form a bimodal pore structure consisting of permeable micropores (0.7 nm < d < 2.0 nm) and ultramicropores (d < 0.7 nm), and thereby facilitated the diffusion of the larger gases through the large micropores, causing a drastic increase in C_3 diffusivity compared to light gases (Table S2). The unprecedented C_3H_6/C_3H_8 selectivity seen in the hybrid CMS membrane was attributed to the tortuous path induced by the impermeable SiO_2 phases created by the thermo-oxidative crosslinking and the subsequent etching of siloxanes which formed additional effective ultramicropores, or to their combination. Thus, while the entirety of our hybrid CMS membranes exceeded the polymeric upper bound, by increasing the SiO_2 phase concentration, the C_3H_6/C_3H_8 separation performance transcended those of previously reported CMS membranes.

Precursor hollow fiber membranes were prepared using the dry-jet/wet-quench process, with the same process parameters detailed in our previous work [16]. Single gas permeation results for C_3H_6 and C_3H_8 for both the precursor and

FEEDBACK

fiber membrane are summarized in Table 2. The PI-LPSQ20 hollow fiber membrane (PI-LPSQ20 HFM) showed a slightly higher C_3H_6/C_3H_8 selectivity compared to that of the dense film (i.e., 13 vs 12), which can be attributed to rheologically induced molecular orientation during the extrusion process [33]. The corresponding CMS PI-LPSQ20 HFM aged 30 days after pyrolyzing, however, failed to display a higher C_3H_6/C_3H_8 selectivity compared to the CMS dense films (i.e., 57 vs. 67) probably because the molecular orientation in precursor hollow fiber membranes was lost in the CMS hollow fibers with the formation of a sp2 hybridized carbon structure. Also, it showed a moderate C_3H_6 permeance of 2.9 GPU due to the detrimental physical aging. Nevertheless, the measured C_3H_6/C_3H_8 ideal selectivity was 57, demonstrating that the superior C_3H_6/C_3H_8 separation properties attained by the thermo-oxidative crosslinking and subsequent etching of double-stranded siloxanes were successfully translated into the hollow fiber form.

Table 2. Single gas permeation results of hybrid precursor hollow fiber membranes and hybrid CMS hollow fiber membranes at *ca.* 1 bar, 35 °C.

Sample	P_{C3H6} [a)]	P_{C3H8} [a)]	$\alpha_{C3H6/C3H8}$ (–)
PI-LPSQ20 HFM	3.3	0.30	13
CMS PI-LPSQ20 HFM (aged 30 days)	2.9	0.05	57

a Permeance in GPU, where 1 GPU = 10^{-6} cm^3(STP) cm^{-2} s^{-1} $cmHg^{-1}$.

Adsorption isotherms of both gases in each CMS membrane were measured at 35 °C (Fig. 3) with the corresponding Langmuir model parameters (Table 3) in order to probe the C_3H_6 and C_3H_8 permeability trends into two factors (i.e., solubility and diffusivity) [34]. As represented in Table 3, the Langmuir affinity constant, *b* of CMS membranes for C_3H_6 increased with increasing concentration of inorganic phases due to the interaction between polar hydroxyl groups on the evenly distributed SiO_2 phases and the polar nature of C_3H_6 [35]. Also, the reduction in Langmuir hole filling capacity (C_H') with increasing concentration of inorganic phases derived from LPSQ in hybrid CMS membranes indicated that the micropore volumes available for C_3H_6 and C_3H_8 gas molecules to access, are diminished, resulting in the solubility decrease. As shown in Fig. S3, the solubility selectivity of C_3H_6/C_3H_8 is minimal, approximately 1.2 for all three different CMS membranes due to their comparable condensability (T_c of C_3H_6 = 225 K vs. T_c of C_3H_8 = 231 K). The diffusivity selectivity, however, increased from 11 to 56 as the LPSQ concentration increased, drastically enhancing the C_3H_6/C_3H_8 permselectivity of hybrid CMS membranes. These results are in agreement with our initial hypothesis and pore size distribution results; the etching of non-porous inorganic phases at a certain temperature evolves particular-sized ultramicropores, since the ultramicropores generated from inorganic phases were highly selective to C_3H_6/C_3H_8 separation but non-selective to CO_2/N_2 separation. However, it is also feasible to include the possibility that the SiO_2 phases might create a tortuous path for C_3H_6 and C_3H_8, causing a decrease in C_3H_6 and C_3H_8 diffusivity while improving the C_3H_6/C_3H_8 diffusivity selectivity.

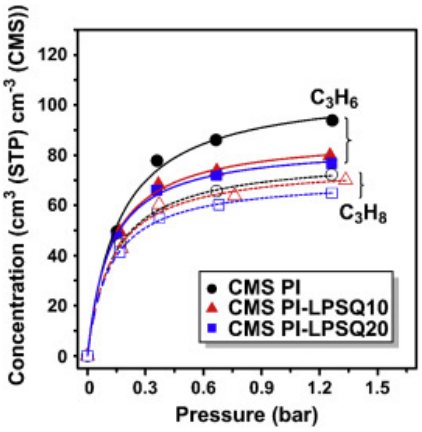

Download : Download high-res image (247KB) Download : Download full-size image

FEEDBACK

Fig. 3. Equilibrium adsorption isotherms for C_3H_6 and C_3H_8 of CMS membranes at 35 °C.

Table 3. Langmuir model parameters for C_3H_6 and C_3H_8 in CMS membranes at 35 °C.

Samples	Gas	C_H' (cm^3(STP) cm^{-3}(CMS))	b (bar^{-1})
CMS PI	C_3H_6	107 ± 4	6.2 ± 0.9
	C_3H_8	80 ± 1	7.5 ± 0.2
CMS PI-LPSQ10	C_3H_6	88 ± 2	8.2 ± 0.9
	C_3H_8	77 ± 3	6.5 ± 0.6
CMS PI-LPSQ20	C_3H_6	84 ± 2	8.9 ± 0.8
	C_3H_8	71 ± 1	8.6 ± 0.5

Note: The error bars were estimated using the least square method [32].

3.3. Mixed gas separation performance

Furthermore, the permeation tests for C_3H_6/C_3H_8 binary gas mixtures (50/50 mol/mol) were conducted at 35 °C and a C_3H_6 partial pressure of *ca.* 1 bar on CMS membranes carbonized at 675 °C. As shown in Table 4, the mixed gas C_3H_6/C_3H_8 separation performances were lower than those of single gas, but still comparable to those of the best performing CMS membranes reported to date (Fig. 4). The bulk effect facilitated C_3H_8 transport and precipitated a depression in the C_3H_6/C_3H_8 separation factors compared with the ideal selectivity of single gases [36]. In addition, it was the negative coupling in simultaneous sorption of C_3H_6 and C_3H_8 gases that attenuated the C_3H_6 permeabilities of CMS membranes as discussed in other studies [37]. Nevertheless, the CMS PI-LPSQ20 membranes still exhibited an excellent separation factor of 52 for C_3H_6/C_3H_8 mixed gas permeation tests and eclipsed the required C_3H_6/C_3H_8 separation performance for commercial application (Fig. 4). Also, the CMS PI-LPSQ20 HFM aged a week after pyrolyzing exhibited a good C_3H_6/C_3H_8 separation factor of 35 although it showed a moderate C_3H_6 permeance of 4.1 GPU due to the physical aging.

Table 4. C_3H_6/C_3H_8 equimolar mixed-gas permeation results of CMS membranes at a total pressure of *ca.* 2 bar and 35 °C.

Sample	P_{C3H6}	P_{C3H8}	$\alpha_{C3H6/C3H8}$ (–)
CMS PI[a)]	460 ± 20	45 ± 5	10 ± 1
CMS PI-LPSQ10[a)]	270 ± 80	13 ± 6	22 ± 8
CMS PI-LPSQ20[a)]	67 ± 20	1.6 ± 1	52 ± 20
CMS PI-LPSQ20 HFM (aged 1 week)[b)]	4.1 ± 0.1	0.11 ± 0.01	35 ± 1

Note: The error bars in permeability and permeance were calculated using standard deviation of permeability in at least two separate samples. The error bars in selectivity were estimated using the propagation of uncertainty [32].

a

Permeabilities in Barrer, where 1 Barrer = 10^{-10} cm^3(STP) cm cm^{-2} s^{-1} $cmHg^{-1}$.

FEEDBACK

b)

Permeances in GPU, where 1 GPU = 10^{-6} cm^3(STP) cm^{-2} s^{-1} $cmHg^{-1}$.

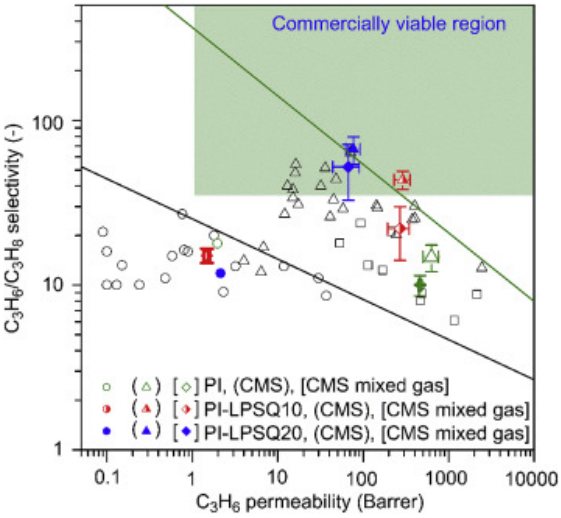

Download : Download high-res image (635KB) Download : Download full-size image

Fig. 4. C_3H_6/C_3H_8 separation performances of polymeric precursor membranes and CMS membranes for single gas as well as mixed gas (50/50 mol/mol) at 35 °C and *ca.* 1 bar. The solid black line indicates the polymeric upper bound for C_3H_6/C_3H_8 separation [38]. The commercially viable region is determined by the minimum C_3H_6 permeability of 1 Barrer and C_3H_6/C_3H_8 selectivity of 35 [39]. The observed trade-off between C_3H_6 permeability and C_3H_6/C_3H_8 selectivity seen in CMS membranes is indicated by the solid green line. Open circle: polymeric membranes [3,38,[40], [41], [42], [43]], open triangle: CMS membranes [7,15,23,34,[44], [45], [46], [47], [48], [49], [50]], open square: hybrid silica membranes [51,52]. The error bars in permeability were calculated using standard deviation of permeability in at least two separate samples. The error bar in selectivity were estimated using the propagation of uncertainty [32]. (For interpretation of the references to colour in this figure legend, the reader is referred to the Web version of this article.)

3.4. Techno-economic analysis

To investigate the economic feasibility of the proposed membrane in comparison with conventional distillation column, we developed a hybrid process for the separation of C_3H_6 from the effluent mixture of C_3H_8 dehydrogenation reactor by integrating two membranes with a distillation column as shown in Fig. 5 [53,54]. (see Tables S3 and S4 for more details about stream information). It should be noted that the optimal location of the membrane can vary depending on the membrane characteristics [55,56], and our preliminary studies (Table S6) revealed that the "membrane followed by distillation column" scheme is more economical than the "distillation column followed by membrane" analogue as reported by other studies [52]. The process model was developed based on experimental data, using two commercial process simulators, i.e., Aspen Plus (for distillation column) and MATLAB (for membrane). The processing rate (1200 tons of C_3H_6/C_3H_8 mixtures per day) [57] and feed condition (C_3H_6: C_3H_8 = 9:1 M ratio, 35 °C, 14 bar) were taken from previous reports [58,59]. The unit equipment costs were estimated using Aspen Process Economic Analyzer [[60], [61], [62]]. All equipment and material costs were adjusted to a common basis year of 2016 [63]. A detailed description of the economic parameters and assumptions are provided in Supplementary Material.

FEEDBACK

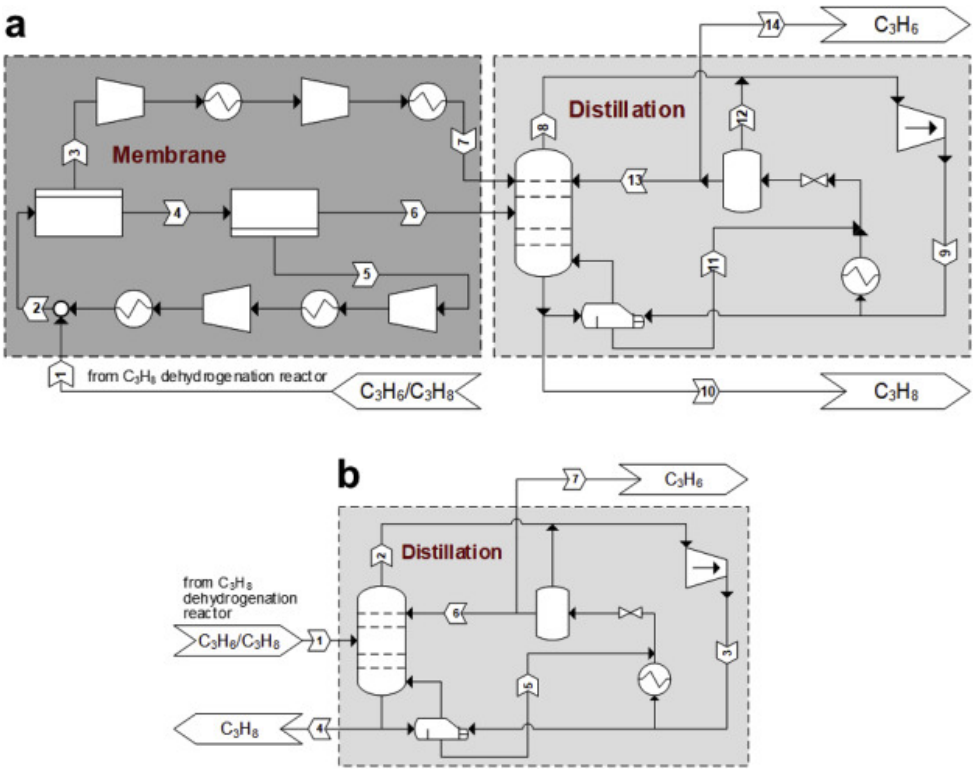

Download : Download high-res image (496KB) Download : Download full-size image

Fig. 5. Process flow diagram. (a) Hybrid (membrane + distillation) process. (b) Distillation-only process.

Fig. 6 shows the total cost breakdown of the hybrid processes with three different membranes and a comparison with the conventional distillation-only process. The lowest total cost is \$20.5/ton-C_3H_6 for the hybrid process with CMS PI-LPSQ20. Compared to the hybrid processes with CMS PI and CMS PI-LPSQ10, the total cost of the hybrid process with CMS PI-LPSQ20 is reduced due to higher C_3H_6/C_3H_8 selectivity of the membrane, leading to a decrease in the subsequent distillation cost by more than 23.6–44.2%. The total cost of the hybrid process with CMS PI-LPSQ20 is 13.1% lower than that of the distillation-only process primarily because it has smaller distillation resulting from smaller reflux rate (335.2 ton/h vs. 211.2 ton/h), and smaller column diameter (7.4 m vs. 5.1 m), which outweighs the capital and operating costs of the additional membranes. The total cost of the hybrid process with CMS PI-LPSQ20 is also lower than that of the hybrid process with ZIF-8 mainly due to a lower material cost, despite a lower C_3H_6/C_3H_8 separation performance [50].

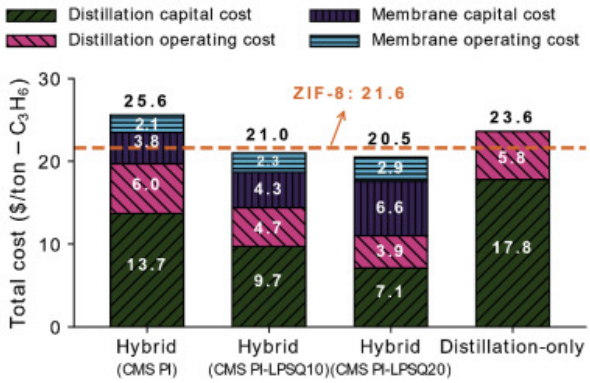

Download : Download high-res image (389KB) Download : Download full-size image

Fig. 6. Total cost components for different C_3H_6/C_3H_8 separation processes.

FEEDBACK

Fig. 7 shows the effect of membrane performance (C_3H_6/C_3H_8 selectivity and C_3H_6 permeance) on the total cost. In these calculations, the membrane selectivity was varied for membranes with C_3H_6 permeances of 2.9, 8.7, and 29.0 GPU. At C_3H_6/C_3H_8 selectivities of less than 30, the total cost is a strong function of membrane selectivity. For example, as the C_3H_6/C_3H_8 selectivity increases from 10 to 30, the total cost decreases from \$43.3/ton-C_3H_6 to \$22.5/ton-C_3H_6 for a 2.9 GPU C_3H_6 membrane. However, at selectivities above 30, the total cost remains almost constant regardless of the C_3H_6/C_3H_8 selectivity, and the enhancement in C_3H_6 permeance is more critical than the selectivity enhancement from the economic point of view. This is because increasing C_3H_6 permeance leads to smaller membrane area and thus smaller capital cost, while increasing selectivity has only a small impact on product purity, which is associated with power requirement.

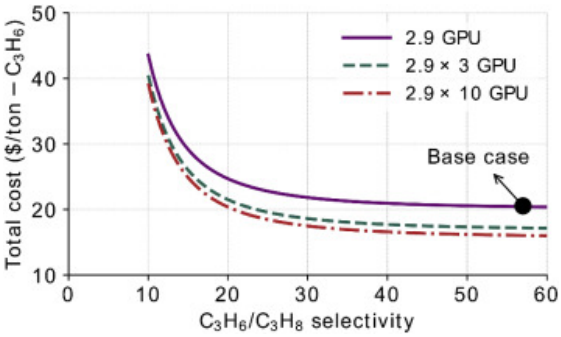

Download : Download high-res image (192KB) Download : Download full-size image

Fig. 7. Sensitivity of the total cost with respect to C_3H_6/C_3H_8 selectivity and C_3H_6 permeance.

Fig. 8 shows how the total cost changes with membrane cost for the membrane lifetime of 5 and 10 yrs. For the membrane lifetime of 5 yr, if the membrane cost is less than \$81.1/m^2, the hybrid process is more economical than the distillation-only process, while the distillation-only process is a better option if the membrane cost is higher than \$81.1/m^2. Also, Fig. 8 clearly reveals that the economics of the hybrid process can be improved by increasing the membrane lifetime from 5 to 10 yrs, implying the significance of the long-term stability of membranes.

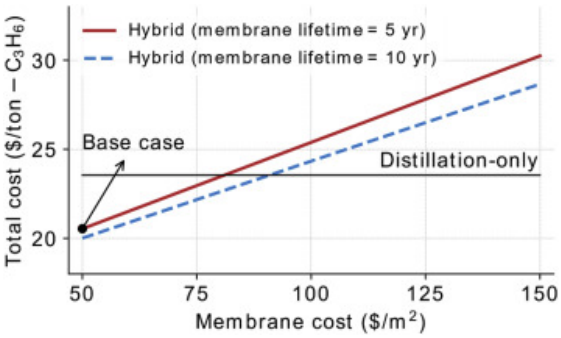

Download : Download high-res image (206KB) Download : Download full-size image

Fig. 8. Sensitivity of the total cost with respect to membrane cost and membrane lifetime.

4. Conclusions

In summary, we investigated the effect of thermo-oxidative crosslinking of siloxane in PI/LPSQ CMS membranes on gas separation performance which was overlooked in the previous study. The HF/CHF_3 gases, derived from the fluo

FEEDBACK

induced the partial etching of SiO_2 in the hybrid CMS membranes, enhancing the formation of effective ultramicropores for C_3H_6/C_3H_8 separation as seen from the DFT-based pore size distribution. With structural characterization, our thorough transport analyses suggested the existence of a tortuous path created from the remnant SiO_2, which is supported by the 6-fold increase in C_3H_6/C_3H_8 diffusivity selectivity as well as C_3H_6 diffusivity loss compared to the bare CMS PI membrane. Also, our hybrid CMS membranes exhibited promising C_3H_6/C_3H_8 separation performance in C_3H_6/C_3H_8 (50/50 mol/mol) mixed feed conditions, especially with an exceptional C_3H_6/C_3H_8 separation factor of 52. Finally, techno-economic analyses showed that the total cost of operating a hybrid process (membrane followed by distillation) for C_3H_6/C_3H_8 separation was 13.1% lower than the conventional distillation-only process. In addition, they demonstrated the significance of permeability and lifetime of membranes for the economical C_3H_6/C_3H_8 separation process based on some case studies.

Declaration of competing interest

The authors declare that they have no known competing financial interests or personal relationships that could have appeared to influence the work reported in this paper.

Acknowledgment

This work was supported by the National Research Foundation of Korea (NRF) grant funded by the Korea government (MSIP) (No. 2017R1A2B4007987) and the "Next Generation Carbon Upcycling Project" (Project No.2018M1A2A6075919) through the National Research Foundation of Korea (NRF) funded by the Ministry of Science and ICT, Republic of Korea.

Appendix A. Supplementary data

The following is the Supplementary data to this article:

Download : **Download Word document (392KB)**

Multimedia component 1.

Recommended articles Citing articles (5)

References

[1] K.M. Steel, W.J. Koros
Investigation of porosity of carbon materials and related effects on gas separation properties
Carbon, 41 (2003), pp. 253-266, 10.1016/S0008-6223(02)00309-3
Article Download PDF View Record in Scopus Google Scholar

[2] M.C. Campo, F.D. Magalhães, A. Mendes
Comparative study between a CMS membrane and a CMS adsorbent: Part I—morphology, adsorption equilibrium and kinetics
J. Membr. Sci., 346 (2010), pp. 15-25, 10.1016/j.memsci.2009.08.045
Article Download PDF View Record in Scopus Google Scholar

[3] K.M. Steel, W.J. Koros
An investigation of the effects of pyrolysis parameters on gas separation properties of carbon materials
Carbon, 43 (2005), pp. 1843-1856, 10.1016/j.carbon.2005.02.028
Article Download PDF View Record in Scopus Google Scholar

[4] S.M. Saufi, A.F. Ismail
Fabrication of carbon membranes for gas separation—a review
Carbon, 42 (2004), pp. 241-259, 10.1016/j.carbon.2003.10.022

FEEDBACK

Article Download PDF View Record in Scopus Google Scholar

[5] X. Ning, W.J. Koros
Carbon molecular sieve membranes derived from Matrimid® polyimide for nitrogen/methane separation
Carbon, 66 (2014), pp. 511-522, 10.1016/j.carbon.2013.09.028
Article Download PDF View Record in Scopus Google Scholar

[6] M. Kiyono, P.J. Williams, W.J. Koros
Effect of pyrolysis atmosphere on separation performance of carbon molecular sieve membranes
J. Membr. Sci., 359 (2010), pp. 2-10, 10.1016/j.memsci.2009.10.019
Article Download PDF View Record in Scopus Google Scholar

[7] S. Fu, G.B. Wenz, E.S. Sanders, S.S. Kulkarni, W. Qiu, C. Ma, W.J. Koros
Effects of pyrolysis conditions on gas separation properties of 6FDA/DETDA:DABA(3:2) derived carbon molecular sieve membranes
J. Membr. Sci., 520 (2016), pp. 699-711, 10.1016/j.memsci.2016.08.013
Article Download PDF View Record in Scopus Google Scholar

[8] H.C. Lee, M. Monji, D. Parsley, M. Sahimi, P. Liu, F. Egolfopoulos, T. Tsotsis
Use of steam activation as a post-treatment technique in the preparation of carbon molecular sieve membranes
Ind. Eng. Chem. Res., 52 (2013), pp. 1122-1132, 10.1021/ie300261r
CrossRef View Record in Scopus Google Scholar

[9] H. Richter, H. Voss, N. Kaltenborn, S. Kämnitz, A. Wollbrink, A. Feldhoff, J. Caro, S. Roitsch, I. Voigt
High-flux carbon molecular sieve membranes for gas separation
Angew. Chem. Int. Ed., 56 (2017), pp. 7760-7763, 10.1002/anie.201701851
CrossRef View Record in Scopus Google Scholar

[10] Y.H. Chu, D. Yancey, L. Xu, M. Martinez, M. Brayden, W. Koros
Iron-containing carbon molecular sieve membranes for advanced olefin/paraffin separations
J. Membr. Sci., 548 (2018), pp. 609-620, 10.1016/j.memsci.2017.11.052
Article Download PDF View Record in Scopus Google Scholar

[11] O. Salinas, X. Ma, E. Litwiller, I. Pinnau
High-performance carbon molecular sieve membranes for ethylene/ethane separation derived from an intrinsically microporous polyimide
J. Membr. Sci., 500 (2016), pp. 115-123, 10.1016/j.memsci.2015.11.013
Article Download PDF View Record in Scopus Google Scholar

[12] J. Liu, Y. Xiao, T.S. Chung
Flexible thermally treated 3D PIM-CD molecular sieve membranes exceeding the upper bound line for propylene/propane separation
J. Mater. Chem. A., 5 (2017), pp. 4583-4595, 10.1039/C6TA09751K
CrossRef View Record in Scopus Google Scholar

[13] X. Zhang, W. Zhu, H. Liu, T. Wang
Novel tubular composite carbon-zeolite membranes
Mater. Lett., 58 (2004), pp. 2223-2226, 10.1016/j.matlet.2004.01.027
Article Download PDF View Record in Scopus Google Scholar

[14] P.S. Tin, Y. Xiao, T. Chung
Polyimide-carbonized membranes for gas separation: Structural, composition, and morphological control of precursors
Separ. Purif. Rev., 35 (2006), pp. 285-318, 10.1080/15422110601003481
CrossRef View Record in Scopus Google Scholar

[15] H.B. Park, Y.M. Lee

FEEDBACK

Fabrication and characterization of nanoporous carbon/silica membranes
Adv. Mater., 17 (2005), pp. 477-483, 10.1002/adma.200400944
CrossRef View Record in Scopus Google Scholar

[16] J.H. Shin, H.J. Yu, H. An, A.S. Lee, S.S. Hwang, S.Y. Lee, J.S. Lee
Rigid double-stranded siloxane-induced high-flux carbon molecular sieve hollow fiber membranes for CO_2/CH_4 separation
J. Membr. Sci. (2019), pp. 504-512, 10.1016/j.memsci.2018.10.076
570–571
Article Download PDF View Record in Scopus Google Scholar

[17] N. Bhuwania, Y. Labreche, C.S.K. Achoundong, J. Baltazar, S.K. Burgess, S. Karwa, L. Xu, C.L. Henderson, P.J. Williams, W.J. Koros
Engineering substructure morphology of asymmetric carbon molecular sieve hollow fiber membranes
Carbon, 76 (2014), pp. 417-434, 10.1016/j.carbon.2014.05.008
Article Download PDF View Record in Scopus Google Scholar

[18] O. Sanyal, S.T. Hicks, N. Bhuwania, S. Hays, M.G. Kamath, S. Karwa, R. Swaidan, W.J. Koros
Cause and effects of hyperskin features on carbon molecular sieve (CMS) membranes
J. Membr. Sci., 551 (2018), pp. 113-122, 10.1016/j.memsci.2018.01.021
Article Download PDF View Record in Scopus Google Scholar

[19] M.R. Kosuri, W.J. Koros
Defect-free asymmetric hollow fiber membranes from Torlon®, a polyamide–imide polymer, for high-pressure CO_2 separations
J. Membr. Sci., 320 (2008), pp. 65-72, 10.1016/j.memsci.2008.03.062
Article Download PDF View Record in Scopus Google Scholar

[20] P. Tarazona, U.M.B. Marconi, R. Evans
Phase equilibria of fluid interfaces and confined fluids
Mol. Phys., 60 (1987), pp. 573-595, 10.1080/00268978700100381
CrossRef View Record in Scopus Google Scholar

[21] W.J. Koros, D.R. Paul
Design considerations for measurement of gas sorption in polymers by pressure decay
J. Polym. Sci. Polym. Phys. Ed, 14 (1976), pp. 1903-1907, 10.1002/pol.1976.180141014
CrossRef Google Scholar

[22] C. Zhang, W.J. Koros
Ultraselective carbon molecular sieve membranes with tailored synergistic sorption selective properties
Adv. Mater., 29 (2017), p. 1701631, 10.1002/adma.201701631
CrossRef View Record in Scopus Google Scholar

[23] M.L. Chng, Y. Xiao, T.S. Chung, M. Toriida, S. Tamai
Enhanced propylene/propane separation by carbonaceous membrane derived from poly (aryl ether ketone)/2,6-bis(4-azidobenzylidene)-4-methyl-cyclohexanone interpenetrating network
Carbon, 47 (2009), pp. 1857-1866, 10.1016/j.carbon.2009.03.032
Article Download PDF View Record in Scopus Google Scholar

[24] L.N. Krasnoperov, J.T. Niiranen, D. Gutman, C.F. Melius, M.D. Allendorf
Kinetics and thermochemistry of $Si(CH_3)_3$ + NO reaction: direct determination of a Si-N bond energy
J. Phys. Chem., 99 (1995), pp. 14347-14358, 10.1021/j100039a023
CrossRef View Record in Scopus Google Scholar

[25] M.L. Huggins

FEEDBACK

Bond energies and polarities
J. Am. Chem. Soc., 75 (1953), pp. 4123-4126, 10.1021/ja01113a001
CrossRef View Record in Scopus Google Scholar

[26] W. Qiu, C.C. Chen, L. Xu, L. Cui, D.R. Paul, W.J. Koros
Sub-T_g cross-linking of a polyimide membrane for enhanced CO_2 plasticization resistance for natural gas separation
Macromolecules, 44 (2011), pp. 6046-6056, 10.1021/ma201033j
CrossRef View Record in Scopus Google Scholar

[27] M. Kiyono, P.J. Williams, W.J. Koros
Effect of polymer precursors on carbon molecular sieve structure and separation performance properties
Carbon, 48 (2010), pp. 4432-4441, 10.1016/j.carbon.2010.08.002
Article Download PDF View Record in Scopus Google Scholar

[28] P. Ho, J.E. Johannes, R.J. Buss, E. Meeks
Modeling the plasma chemistry of C_2F_6 and CHF_3 etching of silicon dioxide, with comparisons to etch rate and diagnostic data
J. Vac. Sci. Technol. A, 19 (2001), pp. 2344-2367, 10.1116/1.1387048
View Record in Scopus Google Scholar

[29] W. Qiu, L. Xu, C.C. Chen, D.R. Paul, W.J. Koros
Gas separation performance of 6FDA-based polyimides with different chemical structures
Polymer, 54 (2013), pp. 6226-6235, 10.1016/j.polymer.2013.09.007
Article Download PDF View Record in Scopus Google Scholar

[30] S. Park, A.S. Lee, Y.S. Do, J.F. Kim, S.S. Hwang, Y.M. Lee, J.H. Lee, J.S. Lee
Side-chain engineering of ladder-structured polysilsesquioxane membranes for gas separations
J. Membr. Sci., 516 (2016), pp. 202-214, 10.1016/j.memsci.2016.06.016
Article Download PDF View Record in Scopus Google Scholar

[31] W. Qiu, K. Zhang, F.S. Li, K. Zhang, W.J. Koros
Gas separation performance of carbon molecular sieve membranes based on 6FDA-mPDA/DABA (3:2) polyimide
ChemSusChem, 7 (2014), pp. 1186-1194, 10.1002/cssc.201300851
CrossRef View Record in Scopus Google Scholar

[32] P.R. Bevington, K.D. Robinson
Data Reduction and Error Analysis for the Physical Sciences
McGraw Hill, Boston (2003)
Google Scholar

[33] A.F. Ismail, S.J. Shilton, I.R. Dunkin, S.L. Gallivan
Direct measurement of rheologically induced molecular orientation in gas separation hollow fibre membranes and effects on selectivity
J. Membr. Sci., 126 (1997), pp. 133-137, 10.1016/S0376-7388(96)00274-8
Article Download PDF View Record in Scopus Google Scholar

[34] K. Okamoto, S. Kawamura, M. Yoshino, H. Kita, Y. Hirayama, N. Tanihara, Y. Kusuki
Olefin/paraffin separation through carbonized membranes derived from an asymmetric polyimide hollow fiber membrane
Ind. Eng. Chem. Res., 38 (1999), pp. 4424-4432, 10.1021/ie990209p
View Record in Scopus Google Scholar

[35] S.M. Davoodi, M. Sadeghi, M. Naghsh, A. Moheb
Olefin–paraffin separation performance of polyimide Matrimid®/silica nanocomposite membranes
RSC Adv., 6 (2016), pp. 23746-23759, 10.1039/C6RA00553E

FEEDBACK

CrossRef View Record in Scopus Google Scholar

[36] M. Das, W.J. Koros
Performance of 6FDA–6FpDA polyimide for propylene/propane separations
J. Membr. Sci., 365 (2010), pp. 399-408, 10.1016/j.memsci.2010.09.029
Article Download PDF View Record in Scopus Google Scholar

[37] R.J. Swaidan, X. Ma, E. Litwiller, I. Pinnau
Enhanced propylene/propane separation by thermal annealing of an intrinsically microporous hydroxyl-functionalized polyimide membrane
J. Membr. Sci., 495 (2015), pp. 235-241, 10.1016/j.memsci.2015.08.015
Article Download PDF View Record in Scopus Google Scholar

[38] R.L. Burns, W.J. Koros
Defining the challenges for C_3H_6/C_3H_8 separation using polymeric membranes
J. Membr. Sci., 211 (2003), pp. 299-309, 10.1016/S0376-7388(02)00430-1
Article Download PDF View Record in Scopus Google Scholar

[39] C.W. Colling, G.A.Jr Huff, J.V. Bartels, Processes Using Solid Perm-Selective Membranes in Multiple Groups for Simultaneous Recovery of Specified Products from a Fluid Mixture, US6830691B2, n.d.
Google Scholar

[40] S.S. Chan, R. Wang, T.S. Chung, Y. Liu
C_2 and C_3 hydrocarbon separations in poly(1,5-naphthalene-2,2′-bis(3,4-phthalic) hexafluoropropane) diimide (6FDA-1,5-NDA) dense membranes
J. Membr. Sci., 210 (2002), pp. 55-64, 10.1016/S0376-7388(02)00374-5
Article Download PDF View Record in Scopus Google Scholar

[41] J.J. Krol, M. Boerrigter, G.H. Koops
Polyimide hollow fiber gas separation membranes: preparation and the suppression of plasticization in propane/propylene environments
J. Membr. Sci., 184 (2001), pp. 275-286, 10.1016/S0376-7388(00)00640-2
Article Download PDF View Record in Scopus Google Scholar

[42] C. Staudt-Bickel, W.J. Koros
Olefin/paraffin gas separations with 6FDA-based polyimide membranes
J. Membr. Sci., 170 (2000), pp. 205-214, 10.1016/S0376-7388(99)00351-8
Article Download PDF View Record in Scopus Google Scholar

[43] K. Tanaka, A. Taguchi, J. Hao, H. Kita, K. Okamoto
Permeation and separation properties of polyimide membranes to olefins and paraffins
J. Membr. Sci., 121 (1996), pp. 197-207, 10.1016/S0376-7388(96)00182-2
Article Download PDF View Record in Scopus Google Scholar

[44] S. Fu
Carbon Molecular Sieve (CMS) Membranes Structure-Property Relationships (PhD Thesis)
Georgia Institute of Technology (2015)
Google Scholar

[45] J. Hayashi, H. Mizuta, M. Yamamoto, K. Kusakabe, S. Morooka, S.H. Suh
Separation of ethane/ethylene and propane/propylene systems with a carbonized BPDA–pp'ODA polyimide membrane
Ind. Eng. Chem. Res., 35 (1996), pp. 4176-4181, 10.1021/ie960264n
View Record in Scopus Google Scholar

[46] M.N. Islam, W. Zhou, T. Honda, K. Tanaka, H. Kita, K. Okamoto

FEEDBACK

Preparation and gas separation performance of flexible pyrolytic membranes by low-temperature pyrolysis of sulfonated polyimides
J. Membr. Sci., 261 (2005), pp. 17-26, 10.1016/j.memsci.2005.02.019
Article Download PDF View Record in Scopus Google Scholar

[47] X. Ma, B.K. Lin, X. Wei, J. Kniep, Y.S. Lin
Gamma-alumina supported carbon molecular sieve membrane for propylene/propane separation
Ind. Eng. Chem. Res., 52 (2013), pp. 4297-4305, 10.1021/ie303188c
CrossRef View Record in Scopus Google Scholar

[48] X. Ma, Y.S. Lin, X. Wei, J. Kniep
Ultrathin carbon molecular sieve membrane for propylene/propane separation
AIChE J., 62 (2016), pp. 491-499, 10.1002/aic.15005
CrossRef View Record in Scopus Google Scholar

[49] C. Karunaweera, I.H. Musselman, K.J. Balkus, J.P. Ferraris
Fabrication and characterization of aging resistant carbon molecular sieve membranes for C_3 separation using high molecular weight crosslinkable polyimide, 6FDA-DABA
J. Membr. Sci., 581 (2019), pp. 430-438, 10.1016/j.memsci.2019.03.065
Article Download PDF View Record in Scopus Google Scholar

[50] R.J. Swaidan, X. Ma, I. Pinnau
Spirobisindane-based polyimide as efficient precursor of thermally-rearranged and carbon molecular sieve membranes for enhanced propylene/propane separation
J. Membr. Sci., 520 (2016), pp. 983-989, 10.1016/j.memsci.2016.08.057
Article Download PDF View Record in Scopus Google Scholar

[51] M. Kanezashi, M. Kawano, T. Yoshioka, T. Tsuru
Organic–inorganic hybrid silica membranes with controlled silica network size for propylene/propane separation
Ind. Eng. Chem. Res., 51 (2012), pp. 944-953, 10.1021/ie201606k
CrossRef View Record in Scopus Google Scholar

[52] M. Kanezashi, W.N. Shazwani, T. Yoshioka, T. Tsuru
Separation of propylene/propane binary mixtures by bis(triethoxysilyl) methane (BTESM)-derived silica membranes fabricated at different calcination temperatures
J. Membr. Sci. (2012), pp. 478-485, 10.1016/j.memsci.2012.05.034
415–416
Article Download PDF View Record in Scopus Google Scholar

[53] J.D. Seader, E.J. Henley, D.K. Roper
Separation Process Principles: Chemical and Biochemical Operations
John Wiley & Sons (2010)
Google Scholar

[54] M. Binns, S. Lee, Y.K. Yeo, J.H. Lee, J.H. Moon, J. Yeo, J.K. Kim
Strategies for the simulation of multi-component hollow fibre multi-stage membrane gas separation systems
J. Membr. Sci., 497 (2016), pp. 458-471, 10.1016/j.memsci.2015.08.023
Article Download PDF View Record in Scopus Google Scholar

[55] A. Motelica, O.S.L. Bruinsma, R. Kreiter, M. den Exter, J.F. Vente
Membrane retrofit option for paraffin/olefin separation—a technoeconomic evaluation
Ind. Eng. Chem. Res., 51 (2012), pp. 6977-6986, 10.1021/ie300587u
CrossRef View Record in Scopus Google Scholar

[56] J. Ploegmakers, A.R.T. Jelsma, A.G.J. van der Ham, K. Nijmeijer

FEEDBACK

Economic evaluation of membrane potential for ethylene/ethane separation in a retrofitted hybrid membrane-distillation plant using unisim design
Ind. Eng. Chem. Res., 52 (2013), pp. 6524-6539, 10.1021/ie400737s
CrossRef View Record in Scopus Google Scholar

[57] H.R. Amedi, M. Aghajani
Economic estimation of various membranes and distillation for propylene and propane separation
Ind. Eng. Chem. Res., 57 (2018), pp. 4366-4376, 10.1021/acs.iecr.7b04169
CrossRef View Record in Scopus Google Scholar

[58] W. Won, K.S. Lee, S. Lee, C. Jung
Repetitive control and online optimization of Catofin propane process
Comput. Chem. Eng., 34 (2010), pp. 508-517, 10.1016/j.compchemeng.2009.12.011
Article Download PDF View Record in Scopus Google Scholar

[59] J.R. Alcántara-Avila, F.I. Gómez-Castro, J.G. Segovia-Hernández, K.I. Sotowa, T. Horikawa
Optimal design of cryogenic distillation columns with side heat pumps for the propylene/propane separation
Chem. Eng. Process, 82 (2014), pp. 112-122, 10.1016/j.cep.2014.06.006
Article Download PDF View Record in Scopus Google Scholar

[60] R. Turton, R.C. Bailie, W.B. Whiting
Analysis, Synthesis and Design of Chemical Processes
Pearson Education (2008)
Google Scholar

[61] W. Won, A.H. Motagamwala, J.A. Dumesic, C.T. Maravelias
A co-solvent hydrolysis strategy for the production of biofuels: process synthesis and technoeconomic analysis
React. Chem. Eng., 2 (2017), pp. 397-405, 10.1039/C6RE00227G
CrossRef View Record in Scopus Google Scholar

[62] J. Lee, Y. Son, S.K. Lee, W. Won
Economic analysis and environmental impact assessment of heat pump-assisted distillation in a gas fractionation unit
Energies, 12 (2019), p. 852, 10.3390/en12050852
CrossRef View Record in Scopus Google Scholar

[63] Plant Cost Index
Chemical Engineering Magazine
n.d.
http://www.che.com/pci/
Google Scholar

[1] These authors contributed equally.

View Abstract

© 2019 Elsevier B.V. All rights reserved.

ELSEVIER
About ScienceDirect
Remote access
Shopping cart
RELX™
FEEDBACK

Advertise

Contact and support

Terms and conditions

Privacy policy

We use cookies to help provide and enhance our service and tailor content and ads. By continuing you agree to the **use of cookies**.
Copyright © 2021 Elsevier B.V. or its licensors or contributors. ScienceDirect ® is a registered trademark of Elsevier B.V.
ScienceDirect ® is a registered trademark of Elsevier B.V.

FEEDBACK